

# Droplets Suspended Beneath a Fiber Hub

Yi Zhang<sup>\*1</sup> and Zhao Pan<sup>\*1</sup>

<sup>1</sup>University of Waterloo, Department of Mechanical and Mechatronics Engineering,  
Waterloo, ON, Canada

March 11, 2025

## Abstract

Droplet-fiber interactions, prevalent in nature and widely applied across various engineering fields, have garnered significant research interest. Many works have focused on the interactions between droplets and single or two fibers. However, the wetting behavior of droplets, especially the maximum droplets that can be retained, on fiber hubs formed by many fibers is rarely studied. The current work explores the capability of fiber hubs to retain liquid droplets. We develop analytical and semi-empirical models to predict the maximum droplet volume on a fiber hub, validating them against experimental data. The variation of maximum volume follows two distinct regimes as the fiber count increases, with a critical fiber number ( $n^* = 32$ ) marking the transition between them. In Regime I ( $n \leq n^*$ ), the volume increases with fiber number, and the stability of a droplet is dictated by the pinning of three-phase contact lines. In Regime II ( $n > n^*$ ), the volume plateaus, with droplets under a fiber hub behaving similarly to those on a flat surface, where the stability is governed by Rayleigh-Taylor instability.

**Key words:** Droplet; Fiber hub; Maximum volume; Three-phase contact line; stability

---

\*To whom correspondence may be addressed: yi.zhang, zhao.pan@uwaterloo.ca

# 1 Introduction

Interactions between droplets and fibers are commonly observed in nature, e.g., raindrops hanging from pine needles [1] and dew droplets on spider webs [2]. They have inspired tremendous applications such as fog harvesting [3, 4], liquid-liquid separation [5], and microfluidic devices [6, 7]. Droplet wetting on thin fiber—‘quasi-one-dimensional’ solid phase—is peculiar and significantly different from that on a flat surface (a two-dimensional interface) due to the geometry of thin cylindrical fibers [8]. Therefore, the physics of droplets interacting with fibers is of great interest (see, for example, [1, 9, 10] among others).

On a single fiber, a droplet can adopt either a barrel or clamshell shape [8]. Chou et al. [11] developed a phase diagram for the droplet’s state in various contact angles and liquid volumes, based on Surface Evolver simulations. For the droplet profile, Wu et al. [12] modeled the morphology of microdroplets on a single fiber, assuming negligible gravity effect. In contrast, Mei et al. [13] examined the influence of gravity on droplet profiles and develop a model for the three-phase contact line (TCL) of barrel-shaped droplets. In addition to droplet profile, the maximum volume of droplets that can be retained by a horizontal fiber [14], by a bent fiber [9], a patterned fiber with periodic spindle knots [4] have also been explored, and the force to detach a droplet from a horizontal fiber is quantified [15]. Furthermore, there are also studies focusing on the interactions between dynamic droplets with a horizontal rigid [14] or flexible fiber [16], and the behaviors of droplets sliding along a tilted or vertical fiber [17, 18].

On two fibers, either in parallel or crossed configuration, droplets behave differently from those on a single fiber. Protiere et al. [19] reported that droplets on two parallel fibers can adopt one of the two states: a liquid drop or a column. A phase diagram for these two states and the transition criteria are developed. Sauret et al. [20] presented that on two crossed fibers, liquid can fully spread into a column or form a drop either in the crossed node or at the end of the column. Moreover, for the two crossed fibers, Gilet et al. [6] and Weyer et al. [7] studied the dynamics of droplets sliding over the intersection, where residual droplets form due to the pinning effect. This pinning effect and controlled residual droplets can be exploited to develop microfluidic devices for drug encapsulation, medical diagnosis, etc. More recently, Khattak et al. [10] reported the directed movement of droplets between two converging fibers towards the apex, demonstrating a novel system for long-distance droplet transport.

However, the wetting behavior of droplets on many fibers—particularly the maximum volume a

droplet can retain at the fibers’ intersections—has been rarely reported in the literature. Droplets suspended from the hub of intersecting fibers, such as the junctions of spider webs [21] and the roots of plants in some hydroponic setups [22], are also commonly observed in nature and industry. Gaining a deeper understanding of these phenomena is not only of academic interest but enables industrial applications. This paper aims to investigate how fiber hubs consisting of varying numbers of fibers retain liquid droplets against gravity.

The rest of this paper is structured as follows. Section 2 introduces the experimental methods for characterizing the maximum droplets of three different liquids hanging from fiber hubs with various number of fibers. Section 3 first presents the experimental results and then develops models predicting the maximum droplet volume. Last, the model is validated against experimental data before concluding the work in section 4.

## 2 Methods

We construct two types of fiber hubs to conduct experiments. The first type composed of 0.5 mm diameter resin fibers in varying numbers ( $n$ , ranging from 1 to 96) is manufactured by 3D printing (EnvisionTEC Pro XL, Germany). The second type is constructed with a circular rigid frame, through which varying numbers ( $n$ ) of 0.1 mm-diameter nylon fibers are stretched, meeting at the center to form a fiber hub.

Three solutions, i.e., 0.01 M and 0.001 M sodium dodecyl sulfate (SDS) solutions, and a mixture of 25 wt% glycerol in water, are used. The surface tensions ( $\gamma$ ) of the three solutions are measured to be 34 mN/m (0.01 M SDS), 44 mN/m (0.001 M SDS), and 67 mN/m (glycerol-water mixture) using the pendant drop method via a contact angle goniometer (Ossila Ltd., UK). The densities ( $\rho$ ) of the three solutions are  $1.00 \times 10^3 \text{ kg/m}^3$  for the two SDS solutions and  $1.06 \times 10^3 \text{ kg/m}^3$  for the glycerol mixture. On a flat resin (the same material with that of the 3D-printed fiber) surface, the contact angles ( $\theta$ ) are  $\sim 6^\circ$  and  $\sim 48^\circ$  for the 0.01 M and 0.001 M SDS solutions, respectively. The contact angle of the glycerol-water mixture on a nylon flat surface is  $\sim 30^\circ$ .

Before experiments, the fiber hubs are rinsed with flowing deionized water, air-dried, and then held horizontally by a support. The solution is first loaded into a syringe, which is connected to a stainless steel needle (gauge 26) positioning just above the fiber hub. The syringe is then driven by a syringe pump (Chemyx Fusion 200, USA) at a low flow rate of 0.5  $\mu\text{L/s}$ , delivering the solution to the fiber hub. A droplet is formed underneath the fiber hub and its volume gradually increases

until it falls, at which point the maximum volume is determined by multiplying the flow rate by the pumping time. The shape of the droplet (the front view) before dropping off is recorded using a high-speed camera (Kron Technologies, Canada). The top view that reveals the three-phase contact lines (TCL) is recorded by a stereo microscope with a magnification ratio of  $40\times$  (AmScope, USA).

### 3 Results and discussion

#### 3.1 Experimental results

Figure 1(A) illustrates the maximum volume of droplets that can be retained beneath fiber hubs as the number of fibers increases. As indicated by the gray triangle symbols, the maximum volume of the glycerol-water mixture droplets increases with the number of nylon fibers up to  $n = 16$ . For  $n > 16$ , despite the fibers being as thin as 0.1 mm in diameter, the stacking height of fibers at the junction reaches  $\sim 2$  mm, which is not negligible for droplets of tens of microliters (radius of  $\sim 2$  mm). In this case, fibers cannot contribute equally to support droplets, and the nylon fiber hubs with  $n > 16$  will not be discussed in this paper. The red square and green circle symbols denote the results for the 0.01 M and 0.001 M SDS solutions, respectively, hanging underneath the 3D-printed fiber hubs. The maximum volume of the droplet first increases with the number of fibers for  $n \leq 32$  and then plateaus for  $n > 32$  for both solutions. Based on these observations, we divide the data in Figure 1(A) into regimes I and II by a critical fiber count  $n^* = 32$ , which will be discussed shortly.

Figure 1(B) and (C) display images of the droplets at their maximum volume suspended from fiber hubs with  $n = 1, 3, 5, 8, 21, 48$ , and a flat surface for the 0.01 M and 0.001 M SDS solutions, respectively. For  $n \leq 32$ , the shape of the droplet varies with the number of fibers. The spreading of droplets along the fiber is enhanced while  $n$  increases (indicated by the escalated length of the green dashed line segments for  $n = 1, 3, 5, 8, 21$ ), while the droplet’s center of mass (COM) remains presumably unchanged. This results in a reduction of the off-axis angle  $\beta$ , which is defined as the angle between the horizontal and the line connecting the COM (indicated by  $O$  in Figure 1(B)) of the droplet and the three-phase point where the fiber exits the droplet. The method for identifying the location of COM can be found in ESI Section 2. For  $n > 32$  (e.g.,  $n = 48$  in (B) and (C)), the droplet shape closely resembles that of a droplet suspended beneath a flat surface. Figure 1(D) shows the variation of  $\beta$  with fiber numbers. For both 0.01 M and 0.001 M SDS solutions,  $\beta$  first decreases and then plateaus as  $n$  increases.

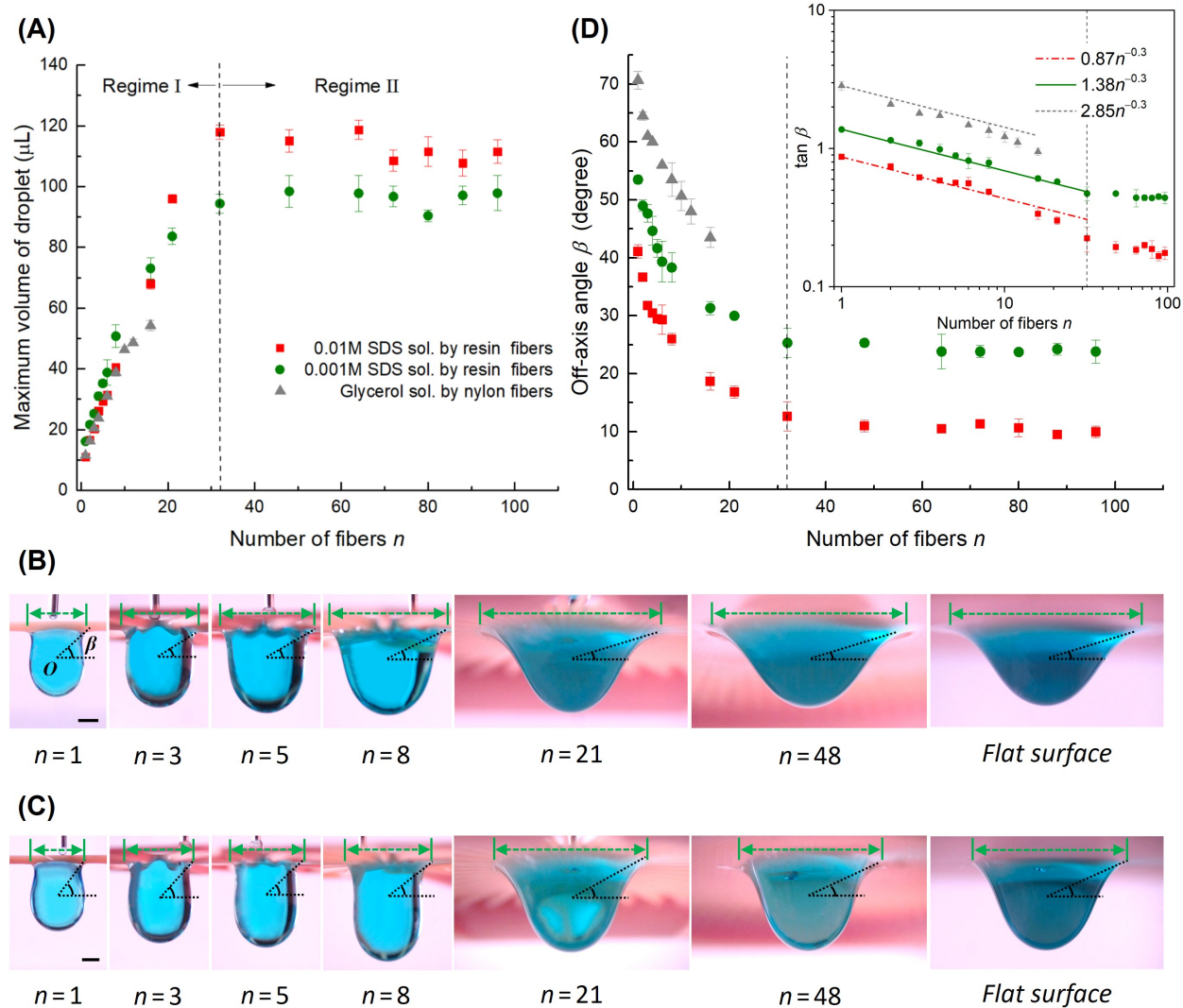


**Figure 1:** (A) Experimental data for the maximum droplet volume with increasing number of fibers (the vertical dashed line represents the critical fiber count  $n^* = 32$ , as also shown in (D)); error bar indicates the standard deviation from the mean of 3–5 measurements; for  $n \geq 48$ , the maximum droplet volume of 0.01 M SDS solution adopts the volume of the bulk droplet, see Electronic Support Information (ESI) Section 1). Photos of maximum droplets for  $n = 1, 3, 5, 8, 21, 48$ , and flat surface for (B) 0.01 M and (C) 0.001 M SDS solutions (scale bar indicates 1 mm; the arrowed line segments indicate the nominal diameter of the wetted area). (D) Variation of off-axis angle  $\beta$  with number of fibers  $n$  (shares legend with (A)).

Figure 2(A-B) and (C) show typical processes of droplets detaching from fiber hubs in regimes I and II, respectively, while Figure 2(D) presents the detachment of a droplet from a flat surface.

In regime I ( $n \leq 32$ ), the stability of droplets is dictated by the pinning of the TCLs. When the droplet reaches its maximum volume, external perturbations can trigger de-pinning of TCLs and the droplet drops off. The de-pinned TCLs are evident by observing the shrinking line segments as shown in Figure 2(A-B). The three-phase contact points move inwards along the fibers and then the droplet detaches due to a pinch-off close to the fiber hub. In regime II ( $n > 32$ ), the mechanism of droplet dropping off from a fiber hub is similar to that on flat surfaces. When a droplet exceeds its critical volume, the TCL overall remains pinned, while the detachment is instead mainly driven by necking, which is similar to the observation for Rayleigh-Taylor instability [23]. As shown in Figure 2(C-D), the arrowed line segments indicating the pinned TCLs remain almost unchanged as the droplet begins to elongate downward. A neck then forms, progressively separating the droplet into two parts and ultimately leading to drop-off. Note, the pinch off location in this case is much lower than that observed in the experiments for regime I.

## 3.2 Modeling

Based on the experimental data and observations presented in Section 3.1, models for the maximum volume of droplets for the two regimes are established as follows.

### 3.2.1 Regime I

In regime I, where the maximum volume of droplet increases with the number of fibers, the force balance of the droplet is presented in Figure 3 and can be expressed as

$$G = \Omega\rho g = F_{\gamma-end} + F_{\gamma-length}, \quad (1)$$

where  $G$  and  $\Omega$  represent the weight and volume of droplet, respectively;  $\rho$  and  $g$  are the density of liquid and gravitational constant, respectively;  $F_{\gamma-end}$  and  $F_{\gamma-length}$  denote the capillary forces acting at the ends of the wetted portion of the fibers and on the horizontal portion of the fibers, respectively. It should be noted that  $F_{\gamma-length}$  vanishes when the droplet fully wraps the fibers.

At the maximum volume, the TCLs are assumed to consist of partial circles at the ends of the wetted portion of the fibers, connecting by horizontal lines along the fiber. Therefore, the total length of the TCLs is  $4r(\pi/2 + \alpha)$  and  $4l$ , respectively, for each fiber.  $r$  denotes the fiber radius,  $\alpha$  the position angle of TCL along fiber, and  $l$  the exposed length of TCL on a half fiber (see Figure 3 for illustration). The capillary force for a single fiber at the ends of the wetted portion of the fiber,





**Figure 2:** Droplets lose stability and fall down in regime I (A)  $n = 1$  and (B)  $n = 3$ , and regime II (C)  $n = 48$  and (D) flat surface (scale bar indicates 1 mm; the arrowed line segments indicate the nominal diameter of the wetted area, as well as the movement of three-phase contact points).

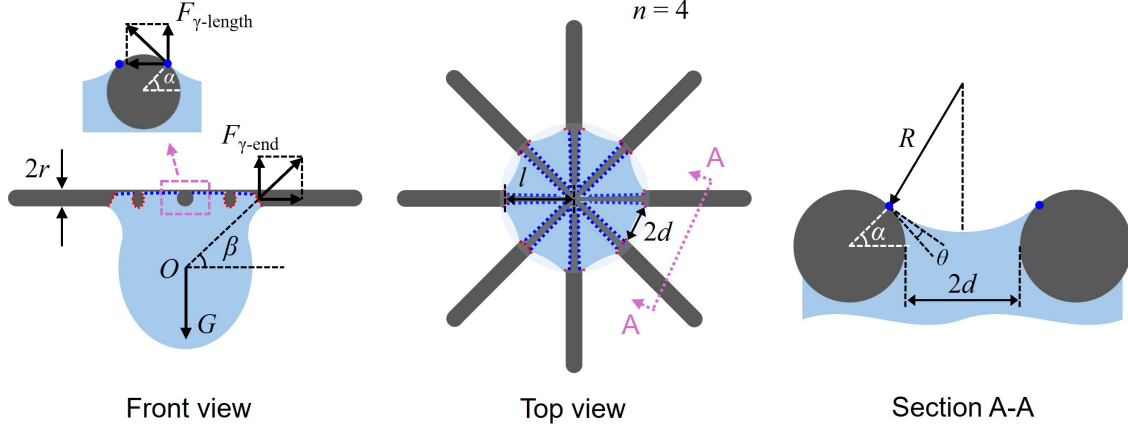


**Figure 3:** Schematic of a droplet hanging under a fiber hub.  $F_{\gamma-end}$  is the capillary force acting at the ends of the wetted portion of the fibers (red dotted lines),  $F_{\gamma-length}$  the capillary force acting on the horizontal portion of the fibers (blue dotted lines),  $G$  the weight of droplet,  $2d$  the distance between fibers at the end of the liquid bridge,  $l$  the exposed length of TCL on a half fiber,  $n$  the number of fiber,  $r$  the radius of fiber,  $R$  the radius of meniscus of the liquid bridge between fibers,  $\alpha$  the position angle of TCL along a fiber,  $\beta$  the off-axis angle,  $\theta$  the contact angle.

$F'_{\gamma-end}$ , can be calculated using (2) based on the model developed by Pan et al. [9]

$$F'_{\gamma-end} \approx 4r \left( \frac{\pi}{2} + \alpha \right) \gamma \cos \theta \tan \beta, \quad (2)$$

where  $\theta$  is the contact angle.  $F_{\gamma-end}$  for the  $n$  fibers can be computed as

$$F_{\gamma-end} = nF'_{\gamma-end}. \quad (3)$$

Similarly,  $F_{\gamma-length}$  for the  $n$  fibers in (12) can be calculated as

$$F_{\gamma-length} \approx 4nl\gamma \cos(\theta + \alpha). \quad (4)$$

Substituting (3) and (4) into (12) gives the maximum volume of the droplet ( $\Omega_I$ ):

$$\Omega_I \approx 4n\lambda^2 \left[ r \cos \theta \tan \beta \left( \frac{\pi}{2} + \alpha \right) + l \cos(\theta + \alpha) \right], \quad (5)$$

where  $\lambda = \sqrt{\frac{\gamma}{\rho g}}$  is the capillary length of the liquid.

Taking  $\Omega_\lambda = \frac{4}{3}\pi\lambda^3$  as characteristic volume of a spherical droplet whose radius is the capillary length, normalizing (5) leads to the non-dimensional maximum volume for regime I:

$$\Omega_I^*(n) = \frac{\Omega_I}{\Omega_\lambda} \approx n \frac{3}{\pi} \left[ r^* \cos \theta \tan \beta \left( \frac{\pi}{2} + \alpha \right) + l^* \cos(\theta + \alpha) \right], \quad \text{for } n \leq 32, \quad (6)$$



where  $r^* = r/\lambda$  and  $l^* = l/\lambda$  are non-dimensional fiber radius and the exposed length, respectively.

By investigating the relationship between  $\beta$  and  $n$ , as shown in the inset of Figure 1(D), we observe a linear correlation between  $\log(\tan \beta)$  and  $\log(n)$  in regime I. Notably, the slopes of the data for various solutions and fibers are nearly identical, approximately  $-0.3$ . This suggests a potential semi-empirical model for  $\beta$  as a function of  $n$ :

$$\tan \beta \approx Cn^{-0.3}, \quad (7)$$

where the  $C = \tan \beta_{n=1}$  and  $\beta_{n=1}$  is the value of  $\beta$  for  $n = 1$  for a given liquid and fiber. In our experiments,  $C = 0.87, 1.38,$  and  $2.85$  for  $0.01$  M SDS,  $0.001$  M SDS, and  $25$  wt% glycerol solutions, respectively.

Furthermore, the geometry in section A-A and the top view of Figure 3 gives

$$\cos(\theta + \alpha) = \frac{r + d - r \cos \alpha}{R} = \frac{l \sin(\frac{\pi}{2n})}{R}, \quad (8)$$

which is also available in exiting literature (see e.g., [20, 24]).  $l \sin(\frac{\pi}{2n})$  in (8) is observed to be  $\lesssim 0.2$  mm in our experiments.  $R$  is close to the droplet radius,  $\sim 2$  mm, leading to an estimate of  $\cos(\theta + \alpha) \lesssim 0.1$ . Accordingly, an approximation of  $\theta + \alpha \approx \pi/2$  can be made to further simplify (6). Substituting (7) and  $\theta + \alpha \approx \pi/2$  into (6) gives

$$\Omega_1^*(n) \approx 3Cn^{0.7}r^* \left(1 - \frac{\theta}{\pi}\right) \cos \theta, \quad \text{for } n \leq 32. \quad (9)$$

Assuming  $\beta$  remains constant at  $\beta_{n=1}$ , meaning that  $\Omega_1^*(n) \approx n\Omega_1^*(n = 1)$ , an asymptote of (9) in the limit of  $n \rightarrow 1$  is given as

$$\Omega_1^*(n) \approx n\Omega_1^*(n = 1) = 3Cnr^* \left(1 - \frac{\theta}{\pi}\right) \cos \theta, \quad \text{for } n \rightarrow 1. \quad (10)$$

Physically, (10) simply evaluates  $\Omega_1^*$  as a function of  $n$  for multiple fibers by scaling  $\Omega_1^*(n = 1)$  for a single fiber by multiplying  $n$ . This practice is expected to overestimate the growth rate of the maximum volume with respect to  $n$ , as it ignored the fact that  $\beta$  decreases with  $n$  in regime I as indicated by (7). As  $n \rightarrow \infty$ ,  $\Omega_1^*$  in (6), (9), or (10) blows up, which is nonphysical. A valid model for  $n \rightarrow \infty$  is needed, which will be presented immediately in the following section.

### 3.2.2 Regime II

The maximum volume of droplet held at the center of the fiber hub plateaus with increasing  $n$ , meaning that the  $\Omega_{II}^*$  is roughly a constant with respect to  $n$  (Figure 1(A)). This observation is

expected as it is natural to view a dense fiber hub as a flat surface in the limit of  $n \rightarrow \infty$ , and the maximum volume of the liquid suspended on the ceiling due to gravity is a classic problem of Rayleigh–Taylor instability [23, 25]. The non-dimensional maximum volume of the droplet hung under a flat surface ( $\bar{\Omega}_\theta^*$ , normalized by  $\Omega_\lambda$ ) before dropping off is a function of the contact angle ( $\theta$ ) of the surface alone. Thus, we expect the maximum volume of the droplet held at the center of a fiber hub approaches  $\bar{\Omega}_\theta^*$  for large  $n$ :

$$\Omega_{\text{II}}^*(n) = \bar{\Omega}_\theta^*, \quad \text{for } n \rightarrow \infty. \quad (11)$$

There is no known analytical solution for  $\bar{\Omega}_\theta^*$ , and only numerical solutions are available, such as the envelope curve developed by Padday and Pitt [25].

In the current work, we use the software Surface Evolver (SE, version 2.70) [26] to simulate the profiles of droplets of increasing volume to determine  $\bar{\Omega}_\theta^*$ . The liquid phase with a specified volume is initialized as a cuboid-shaped slab hanging beneath a flat solid surface of a prescribed contact angle. SE then evolves the liquid cuboid towards its equilibrium shape by minimizing the total free energy (see Section 3 in ESI). We carry out a series of simulations by increasing the volume of the droplet from a small value with an increment of 1  $\mu\text{L}$  until reaching a critical volume, at which a larger droplet detaches from the flat surface.

Figure 4(A) and (B) compare the simulated and actual profiles of the maximum 0.01 M and 0.001 M SDS droplets suspended beneath a flat surface. The simulated profiles by SE closely resemble the image of droplets from experiments. The maximum droplet volumes from simulations and experiments show good agreement. As an additional verification, the model by Padday and Pitt [25] gives 120  $\mu\text{L}$  (calculated by  $\bar{\Omega}_{\theta=6^\circ}^* = 18.6\lambda^3$ , see ESI Section 4) and 96  $\mu\text{L}$  ( $\bar{\Omega}_{\theta=48^\circ}^* = 10.1\lambda^3$ ) for 0.01 M and 0.001 M SDS, respectively. Table 1 summarizes the cross validation of the maximum volume of SDS droplets from the experiments, SE-based simulations, and the results by Padday and Pitt [25].

### 3.3 Validation and discussion

In this section, we validate the models developed in the previous sections for regimes I and II against the experimental data (see Figure 4(C)). In regime I, the analytical model ((6), short dashed lines) and the semi-empirical model ((9), solid lines) predict the maximum droplet volume for different  $n$ , respectively, for the three types of solutions. Both models exhibit good agreement with the experimental data, with a mean relative error of 6.6% and 10.8% for the analytical and

**Table 1:** Cross validation of simulations and experiments for the maximum SDS droplets suspended beneath flat surfaces. The uncertainty (1  $\mu\text{L}$ ) for the Surface Evolver simulations is determined by the incremental volume used in the simulations.

SDS concentration [M]	Maximum volume: $\Omega$ [ $\mu\text{L}$ ]		
	Experiment	Simulation	Padday and Pitt [25]
0.01	$105 \pm 7$	$110 \pm 1$	120
0.001	$93 \pm 4$	$92 \pm 1$	96

semi-empirical models, respectively. In regime II, the model for the maximum volume ((11), dashed lines), adopts the values from the SE-based simulations for  $\bar{\Omega}_\theta^*$  (see also Table 1). The model provides reasonable prediction of the maximum volume for regime II with a mean relative error of 4%.

Figure 4(D) presents Figure 4(C) in logarithmic scale, highlighting the scaling of  $\Omega^*$  with respect to  $n$ . In regime I, the asymptote (10) predicts the maximum volume by multiplying  $\Omega_1^*(n=1)$  for a single fiber by  $n$ , yielding  $\Omega^* \sim n^1$ , resulting in straight dotted lines with a slope of unity. While the maximum volume from experiments, exhibiting strong linearity in logarithmic scale, follows straight solid lines with a slope of 0.7, which rationalizes the prediction by the semi-empirical model (9), i.e.,  $\Omega^* \sim n^1 \tan \beta = n^{0.7}$  for  $n \leq 32$ . The deviation of the experimental maximum volume ( $\Omega^* \sim n^1 \tan \beta$ ) from the asymptote ( $\Omega^* \sim n^1$ ) arises from the reduced off-axis angle ( $\tan \beta \sim n^{-0.3}$ ), leading to a lower growth rate of maximum volume as fiber count increases, see Figure 1(A&D). In regime II, (11) agrees with the experimental data and captures the scaling behavior of  $\Omega^* \sim n^0$  for  $n > 32$ . (10) and (11) can be viewed as two asymptotes for  $\Omega^*(n)$ , in the limits of  $n \rightarrow 1$  (dotted lines) and  $n \rightarrow \infty$  (dashed lines in Figure 4(C&D)), respectively. The intersection of (10) and (11) provides an estimate of the critical fiber number  $n^*$  (however underestimated), yielding  $n^* = 12$  and  $n^* = 10$  for the 0.01 M and 0.001 M SDS solutions, respectively.

## 4 Conclusion

The current work studied the capability of fiber hubs, consisting of  $n = 1$  to 96 fibers, to retain liquid droplets under them. Analytical and semi-empirical models are developed and validated against experimental data. The stability of a droplet and its maximum volume suspended under a

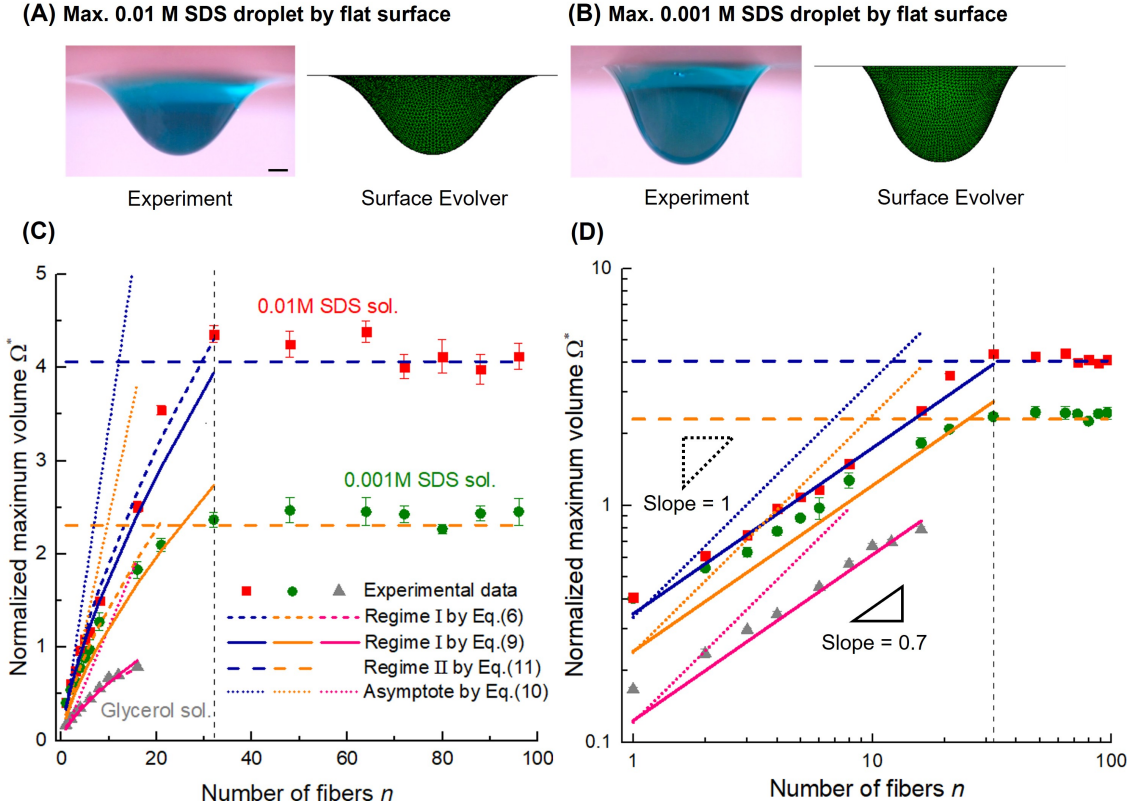


**Figure 4:** The experimental and simulated profiles of the maximum (A) 0.01 M and (B) 0.001 M SDS droplets hanging beneath flat surfaces (scale bar indicates 1 mm). (C) Validation of the analytical model (6), the semi-empirical model (9), and the asymptote (10) for regime I, and the model (11) for regime II against experimental data (the vertical dashed line represents the critical fiber count  $n^* = 32$ , as also shown in (D)). (D) On a logarithmic scale of (C).

fiber hub vary across two distinct regimes, separated by a critical fiber count ( $n^* = 32$ ). In regime I ( $n \leq n^*$ ), the stability of droplets is determined by the pinning of three-phase contact lines, and the maximum volume increases with fiber numbers. However, the growth rate is discounted by the reducing off-axis angle, due to the enhanced spreading of droplets along the fiber. In regime II ( $n > n^*$ ), the maximum volume plateaus with respect to the number of fibers, and the instability is mainly driven by the necking of the droplet. Before detaching, the shape of a droplet suspended beneath a fiber hub closely resembles that of a droplet under a flat surface, with its stability governed by Rayleigh-Taylor instability.

## **Acknowledgement**

The authors would like to express their sincere gratitude for the financial support provided by the Artificial Intelligence for Design Challenge (AI4D) program, funded by the National Research Council Canada.

## Appendix: Supplemental Information

### A Measurement of the maximum volume of the droplet

In our experiments, the fiber hub manufactured by 3D printing consists of fibers with finite thickness meeting at the center of the hub. This results in a grooved disk at the center of the hub. When the number of the fiber is large (e.g.,  $n \geq 48$ ), the diameter of the disk can be large and comparable to the size of the droplet. Outside the disk, the gaps between neighboring fibers are narrow, and can trap a significant amount of liquid.

For example, when measuring the maximum droplet volume of 0.01 M SDS solution underneath the 3D-printed fiber hubs with  $n \geq 48$ , we noticed that, in addition to the bulk droplet hanging under the center of fiber hub, some liquid spread outward from the center of the fiber hub and trapped by the gaps between the fibers.<sup>1</sup> The liquid trapped by the inter-fiber gaps are typically separated from the bulk droplet because the contact area of the bulk droplet (e.g., radius of  $\sim 5$  mm for  $n \geq 48$ ) is often comparable to or smaller than the disk area (e.g., radius exceeding 8 mm for  $n \geq 48$ ). Thus, the bulk liquid is retained within the disk area, while the liquid trapped between the inter-fiber gaps is outside the disk area.

In this case, we count the droplet volume by the volume of the bulk droplet, which is measured by subtracting the liquid volume trapped in the inter-fiber gaps from the total volume of the liquid retained by a fiber hub directly measured using syringe pump (multiplying flow rate by pumping time). The volume of liquid in the gaps is determined by measuring the penetration length along the gaps and integrating the cross-sectional area of the gap (between two adjacent fibers) along this length. Table S2 lists the total volume of the liquid and the volume of the bulk droplet.

**Table S2:** Adjustment of measured volume for 0.01 M SDS solution

Volume of liquid [ $\mu\text{L}$ ]	$n = 48$	$n = 64$	$n = 72$	$n = 80$	$n = 88$	$n = 96$
Direct measurement (bulk droplet and trapped liquid)	$161 \pm 5$	$186 \pm 3$	$182 \pm 5$	$192 \pm 5$	$199 \pm 6$	$211 \pm 5$
bulk droplet	$115 \pm 4$	$119 \pm 3$	$109 \pm 4$	$111 \pm 5$	$108 \pm 4$	$112 \pm 4$

<sup>1</sup>Note, this phenomenon does not happen in the experiments using 0.001 M SDS solution.

## B Identification of the center of mass of a droplet

Figure S5 illustrates a three-step method for determining the center of mass (COM) of the droplet. In Step 1, an image of the droplet is imported into an image processing software, ImageJ. The droplet profile is selected using the “polygon selections” tool, and the coordinates of all the selected points along the profile are extracted. In Step 2, these profile coordinates are imported into a finite element simulation software, COMSOL Multiphysics (version 6.2), where a 3D droplet is generated under the assumption of axisymmetry. The coordinate of COM is then extracted from the “Mass Properties” node in COMSOL. In Step 3, the COM is located and marked on the original photo in ImageJ based on the computed coordinates in Step 2 for further data analysis.

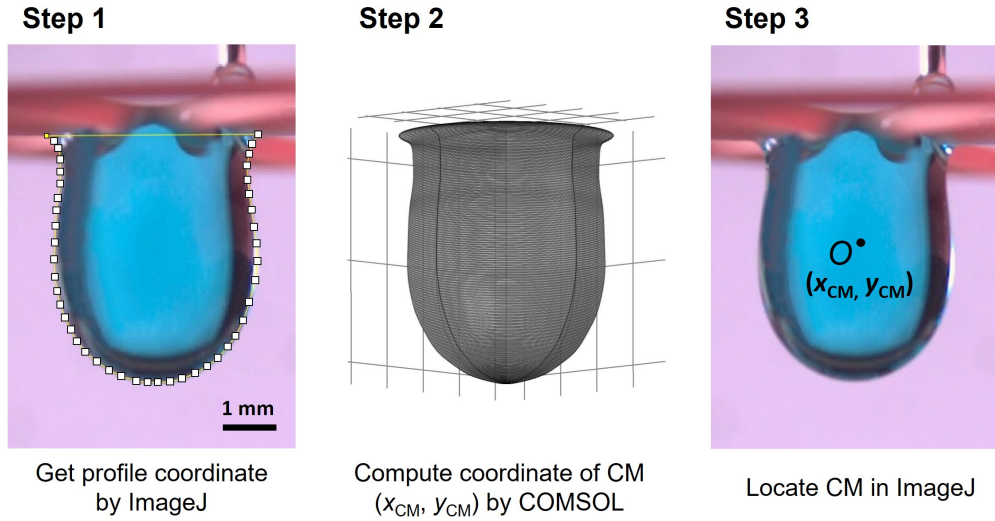


**Figure S5:** Method to identify the center of mass (CM) of the droplet

## C Expression for total free energy

The total free energy attributed to a liquid droplet hanging underneath a flat surface (volume of  $\Omega$  and contact angle  $\theta$ ) is expressed as

$$E(\Omega) = \gamma\Gamma_{LV} - \iint_{\Gamma_{LS}} \gamma \cos \theta d\Gamma - \iiint_{\Omega} \rho g z d\Omega, \quad (12)$$

where  $\Gamma_{LV}$  and  $\Gamma_{LS}$  represent the liquid-vapor and liquid-solid interfacial area, respectively, and the last term denotes the gravitational potential [11]. The profile of the droplet is determined by minimizing (12), which is the governing equation for the Surface Evolver based on simulations.



## D Extracting data from Padday and Pitt (1973)

Figure S6 presents the envelope curve developed by Padday and Pitt [25] to predict the maximum droplet volume beneath a flat surface for various contact angles (denoted by  $\theta$  in the current work and  $\phi$  by Padday and Pitt). For contact angles of  $6^{\text{circ}}$  and  $48^{\text{circ}}$ , the “Figure Calibration” plugin (a digitizer tool) in ImageJ is used to identify points A(6, 18.6) and B(48, 10.1) on the envelope curve, corresponding to the 0.01 M and 0.001 M SDS solutions, respectively. Accordingly, the predicted non-dimensional maximum droplet volumes are  $\Omega_{\theta=6^\circ}^* = 18.6\lambda^3$  and  $\Omega_{\theta=48^\circ}^* = 10.1\lambda^3$  for the 0.01 M and 0.001 M SDS solutions, respectively. In turn, the dimensional maximum volume for these two solutions are  $\Omega = 120 \mu\text{L}$  and  $\Omega = 96 \mu\text{L}$ , respectively.

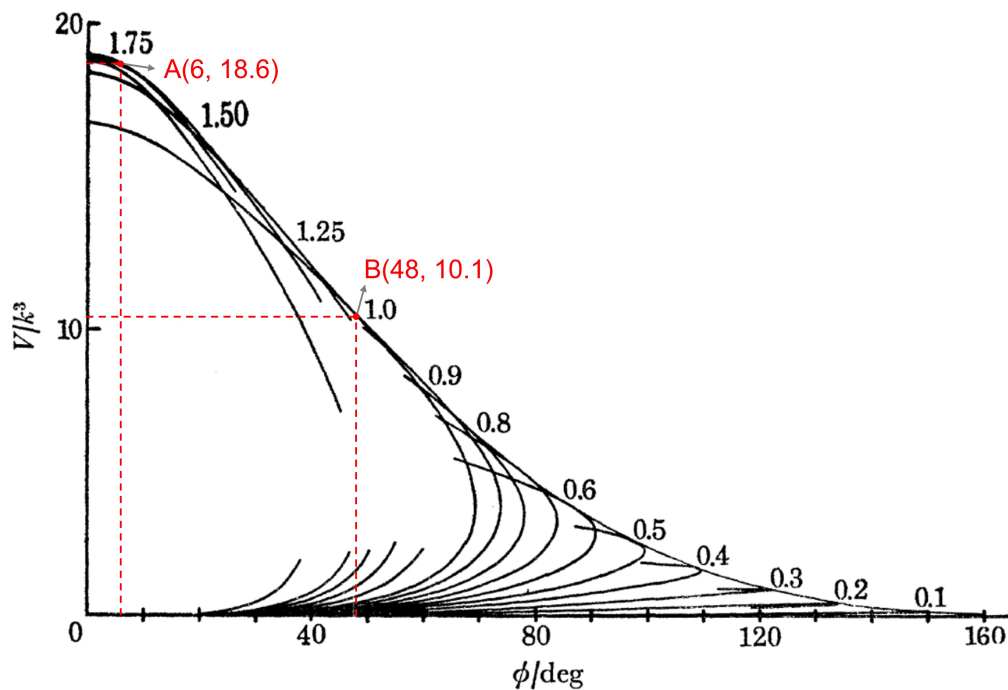


**Figure S6:** The envelope curve developed by Padday and Pitt [25] to predict the maximum droplet volume beneath a flat surface.  $V$ ,  $k$ , and  $\phi$  represent droplet volume, capillary length, and contact angle, respectively.

## References

- [1] C Duprat, S Protiere, AY Beebe, and Howard A Stone. Wetting of flexible fibre arrays. *Nature*, 482(7386):510–513, 2012.

- [2] Yongmei Zheng, Hao Bai, Zhongbing Huang, Xuelin Tian, Fu-Qiang Nie, Yong Zhao, Jin Zhai, and Lei Jiang. Directional water collection on wetted spider silk. *Nature*, 463(7281):640–643, 2010.
- [3] Jie Ju, Hao Bai, Yongmei Zheng, Tianyi Zhao, Ruochen Fang, and Lei Jiang. A multi-structural and multi-functional integrated fog collection system in cactus. *Nature communications*, 3(1):1247, 2012.
- [4] Yongping Hou, Yuan Chen, Yan Xue, Yongmei Zheng, and Lei Jiang. Water collection behavior and hanging ability of bioinspired fiber. *Langmuir*, 28(10):4737–4743, 2012.
- [5] Stuti S Rajgarhia, Sadhan C Jana, and George G Chase. Separation of water from ultralow sulfur diesel using novel polymer nanofiber-coated glass fiber media. *ACS Applied Materials & Interfaces*, 8(33):21683–21690, 2016.
- [6] Tristan Gilet, Denis Terwagne, and Nicolas Vandewalle. Digital microfluidics on a wire. *Applied physics letters*, 95(1), 2009.
- [7] Floriane Weyer, Marjorie Lismont, Laurent Dreesen, and Nicolas Vandewalle. Compound droplet manipulations on fiber arrays. *Soft matter*, 11(36):7086–7091, 2015.
- [8] Glen McHale and MI Newton. Global geometry and the equilibrium shapes of liquid drops on fibers. *Colloids and Surfaces A: Physicochemical and Engineering Aspects*, 206(1-3):79–86, 2002.
- [9] Zhao Pan, Floriane Weyer, William G Pitt, Nicolas Vandewalle, and Tadd T Truscott. Drop on a bent fibre. *Soft Matter*, 14(19):3724–3729, 2018.
- [10] Hamza K Khattak, Aileen Shanzeela, Elie Raphael, and Kari Dalnoki-Veress. Directed droplet motion along thin fibers. *PNAS nexus*, 3(3):pgae086, 2024.
- [11] Tung-He Chou, Siang-Jie Hong, Yu-En Liang, Heng-Kwong Tsao, and Yu-Jane Sheng. Equilibrium phase diagram of drop-on-fiber: coexistent states and gravity effect. *Langmuir*, 27(7):3685–3692, 2011.
- [12] X-F Wu and Yuris A Dzenis. Droplet on a fiber: geometrical shape and contact angle. *Acta mechanica*, 185(3):215–225, 2006.

- [13] Maofei Mei, Jintu Fan, and Dahua Shou. The gravitational effect on the geometric profiles of droplets on horizontal fibers. *Soft Matter*, 9(43):10324–10334, 2013.
- [14] Élise Lorenceau, Christophe Clanet, and David Quéré. Capturing drops with a thin fiber. *Journal of colloid and interface science*, 279(1):192–197, 2004.
- [15] Noor M Farhan and H Vahedi Tafreshi. Universal expression for droplet–fiber detachment force. *Journal of Applied Physics*, 124(7), 2018.
- [16] Emilie Dressaire, Alban Sauret, François Boulogne, and Howard A Stone. Drop impact on a flexible fiber. *Soft matter*, 12(1):200–208, 2016.
- [17] Tristan Gilet, Denis Terwagne, and Nicolas Vandewalle. Droplets sliding on fibres. *The European Physical Journal E*, 31:253–262, 2010.
- [18] Matteo Leonard, Joséphine Van Hulle, Floriane Weyer, Denis Terwagne, and Nicolas Vandewalle. Droplets sliding on single and multiple vertical fibers. *Physical Review Fluids*, 8(10):103601, 2023.
- [19] S Protiere, C Duprat, and Howard A Stone. Wetting on two parallel fibers: drop to column transitions. *Soft Matter*, 9(1):271–276, 2013.
- [20] Alban Sauret, Alison D Bick, Camille Duprat, and Howard A Stone. Wetting of crossed fibers: Multiple steady states and symmetry breaking. *Europhysics Letters*, 105(5):56006, 2014.
- [21] Zhao Qin, Brett G Compton, Jennifer A Lewis, and Markus J Buehler. Structural optimization of 3d-printed synthetic spider webs for high strength. *Nature communications*, 6(1):7038, 2015.
- [22] Imran Ali Lakhari, Jianmin Gao, Tabinda Naz Syed, Farman Ali Chandio, and Noman Ali Buttar. Modern plant cultivation technologies in agriculture under controlled environment: A review on aeroponics. *Journal of plant interactions*, 13(1):338–352, 2018.
- [23] Geoffrey Ingram Taylor. The instability of liquid surfaces when accelerated in a direction perpendicular to their planes. i. *Proceedings of the Royal Society of London. Series A. Mathematical and Physical Sciences*, 201(1065):192–196, 1950.
- [24] HM Princen. Capillary phenomena in assemblies of parallel cylinders: Iii. liquid columns between horizontal parallel cylinders. *Journal of Colloid and Interface Science*, 34(2):171–184, 1970.

[25] JF Padday and AR Pitt. The stability of axisymmetric menisci. *Philosophical Transactions of the Royal Society of London. Series A, Mathematical and Physical Sciences*, 275(1253):489–528, 1973.

[26] Kenneth A Brakke. The surface evolver. *Experimental mathematics*, 1(2):141–165, 1992.